PET (positron emission tomography) imaging of biomolecules using metal–DOTA complexes: a new collaborative challenge by chemists, biologists, and physicians for future diagnostics and exploration of *in vivo* dynamics†

Katsunori Tanaka* and Koichi Fukase

Received 23rd November 2007, Accepted 6th December 2007
First published as an Advance Article on the web 1st February 2008
DOI: 10.1039/b718157b

Recently, PET has been paid a great deal of attention as a non-invasive imaging method. In this review, the recent advances of PET using biomolecules, such as peptides, monoclonal antibodies, proteins, oligonucleotides, and glycoproteins will be described. So far, PET of biomolecules has been mainly used for diagnosis of cancers. The biomolecules have been conjugated with the DOTA ligand, labeled with radiometals as the β^+ emitter, and targeted to specific tumors, where they have enabled visualization of even small metastatic lesions, due to the high sensitivity of the PET scanners. Some of the biomolecules have been used not only for PET diagnosis, but also for radiotherapeutic treatments by simply changing the radiometals to β^- emitters. Collaborative work between chemists, biologists, and physicians will be important for the future of biomolecule-based targeting and diagnosis.

1. Introduction

Positron emission tomography (PET) is an emerging non-invasive method which quantitatively visualizes the locations and levels of radiotracer accumulation with a high imaging contrast.[1] While γ-camera-based scintigraphy such as SPECT (single-photon emission computerized tomography) is limited to a spatial resolution of 12–15 mm, the resolution of current clinical PET scanners is 4–6 mm. In addition, PET is about ten times more sensitive than single-photon based methodologies, thus providing more accurate information on radiotracers accumulated at low levels in tissues. In order to optimize PET tracers in small animal models in advance of clinical applications, the microPET technique has also been developed, and currently gives a volumetric resolution of (1.8 mm)[3]. Corrected data from full three-dimensional emission is combined with an algebraic reconstruction technique, leading to high-definition images of the whole bodies of animals. The increasing availability and lower cost of PET scanners, together with the availability of radiopharmaceuticals, make PET a routine technique for cancer diagnosis even in the clinical field, as well as an important tool in developing new molecular imaging probes that can target specific tissues and in elucidating unexplored biological pathways.

Department of Chemistry, Graduate School of Science, Osaka University, Machikaneyama 1-1, Toyonaka, Osaka 560-0043, Japan. E-mail: ktzenori@chem.sci.osaka-u.ac.jp; Fax: +81(6)68505419

† This paper is dedicated to Professor Nina Berova on the occasion of her significant anniversary and her receiving the Chirality Medal 2007.

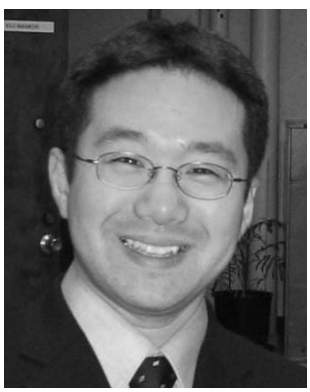

Katsunori Tanaka

Katsunori Tanaka received his Ph.D. (2002) from Kwansei Gakuin University in Japan. After a post-doc at Columbia University, New York (2002–2005), he joined Professor Koichi Fukase's group in Osaka University as an Assistant Professor (2005–present). His research interests include exploring new methods for total synthesis, configurational analysis, biological evaluation, molecular imaging, and molecular recognition of natural products.

Koichi Fukase

Koichi Fukase received his Ph.D. (1987) from Osaka University. Since 1988, he has worked at the Graduate School of Science, Osaka University as a Research Associate (1988), Assistant Professor (1996), Associate Professor (1998), and a full Professor (2004). His research projects are focused on (1) chemistry in innate immunity, (2) carbohydrate chemistry, and (3) molecular imaging.

^{18}F-FDG (2-deoxy-2-[^{18}F]fluoro-D-glucose, Fig. 1) is a Food and Drug Administration-approved radiopharmaceutical, and has become an important PET tracer in detecting primary and metastatic breast, lung and colorectal tumors, melanoma, and lymphoma, as well as monitoring responses to treatment, recurrence, and general prognosis. ^{18}F-FDG is internalized by cells and phosphorylated by hexokinase; due to its highly polar nature, the phosphorylated product cannot diffuse out of cells unless it is dephosphorylated by glucose-6-phosphatase (usually a slow process). Therefore, cancer cells, which generally have an accelerated glycolysis rate and a decreased ability to make energy aerobically, exhibit elevated uptake and retention of ^{18}F-FDG tracer, thus creating a contrast between the tumor-positive tissues and tumor-negative tissues. However, ^{18}F-FDG PET can often be confounded by benign disease as well as by active inflammation, which also exhibits elevated uptake of this tracer, leading to ambiguous conclusions. In order to circumvent such problems of ^{18}F-FDG, a variety of new small-molecule PET probes have been developed.[2–5]

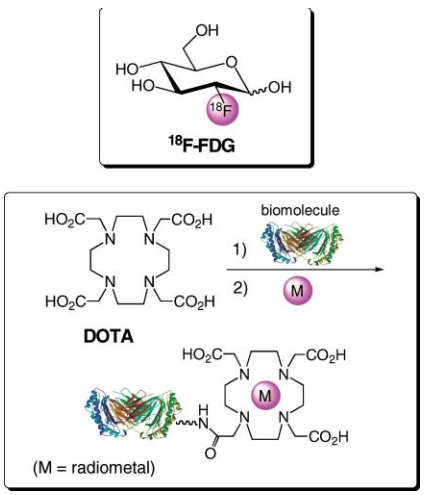

Fig. 1 ^{18}F-FDG and radiometal–DOTA conjugate as a biomolecule-based tracer.

Another interesting possibility for cancer diagnosis is to use biomolecules as molecular imaging probes,[1] since we can easily choose or design desired peptides, proteins, antibodies, and oligonucleotides that exhibit high binding affinity to the target receptors, antigens, and nucleic acids being specifically overexpressed in or on tumor cells. Alternatively, PET imaging of biomolecules can visualize their unknown *in vivo* kinetics where an important biological pathway is involved, which might lead to the discovery of promising biomolecule-based drug candidates. In this review, we would like to survey the recent advances and future perspectives for PET imaging using biomolecules, and discuss the importance of collaborations between chemists, biologists, and physicians for future advances in diagnostic applications and exploration of *in vivo* dynamics.

So far, PET of biomolecules has mainly been used for diagnosis of cancers; therefore, in this review we will focus primarily on these investigations. The best PET tracers for cancer diagnosis must show high and specific affinity to the target receptors which are overexpressed on the tumor cells. These compounds must also be efficiently internalized by tumor cells in order to achieve rapid tumor accumulation at high concentrations, as well as undergoing slow washout *in vivo*. Furthermore, tracers should be rapidly cleared from the blood and exhibit low uptake in the liver and kidney. Co-infusion of L-lysine and/or arginine has been applied to prevent renal accumulation of radioactivity. Stability in the blood is also a very important factor for good tracers; on the other hand, a prolonged biological half-life places the patients in contact with radioactivity for a long time. This is especially true when considering the case of whole antibodies. Therefore, the corresponding small and active portion of an antibody, termed "minibody" has been used as an alternative tracer, and will be discussed in section 4. PET experiments using biomolecules to target specific tumor tissues generally proceed as follows:

(1) The biomolecules, either synthesized, engineered, or isolated from natural sources, are labeled with radiometal ligands. The labeling chemistry is fully optimized in order to efficiently introduce the ligand to the biomolecules, either during solid-phase synthesis of the peptides or by direct labeling of proteins (see section 2). It is very important to attach ligands to biomolecules without inhibiting their activity. DOTA (1,4,7,10-tetraazacyclodecane-1,4,7,10-tetraacetic acid, Fig. 1) is used as the most favorable ligand for biomolecular PET, due to its compatibility with a variety of radiometals and its extremely high stability,[6–11] as well as the favorable clearance properties of the metal complexes *in vivo*.[12] The kinetics and thermodynamic stability of DOTA complexes with a variety of metals, in comparison with other ligands such as EDTA (ethylenediaminetetraacetic acid) or DTPA (diethylenetriaminepentaacetic acid), have been well documented.[12,13] The stability constant for all metals, including the radiometals used for PET imaging, generally follows the order DOTA > DTPA > EDTA, although the metal complexation of DOTA with some lanthanide series metals, such as La^{3+} or Lu^{3+}, is slightly slower than that of EDTA.[12] Although a number of radiometal ligands for imaging, including DTPA, have been reported, this review only focuses on the DOTA ligand, which in our opinion is best suited for PET imaging purposes.

(2) DOTA–biomolecule conjugates are labeled with a variety of radiometals, and their binding affinity to target receptors, antigens, or complementary oligonucleotides are first examined *in vitro*. Tumor cell internalization/externalization is also tested in cell-based assays. The typical radiometals cited in this review are summarized in Table 1. Generally, radiometals with γ-emission are used for SPECT, while β^+ emitters can be used for PET diagnosis. On the other hand, β^- emitters can be specifically used for radiotherapeutic treatments. Some of the radiometals listed in Table 1 are used for both diagnosis and therapeutics. For example, ^{67}Ga has not only been used for SPECT but also for radiotherapy due to its emission of Auger electrons (0.1–8 keV) and conversion electrons (80–90 keV); likewise, ^{68}Ga can be used both for PET and radiotherapy.[14] Since the radiometals introduced into the DOTA ligand show profound effects on the bioproperties of the tracers, the choice of radiometals is critical. Once a DOTA–biomolecule conjugate with a suitable radiometal has been determined *in vitro*, the same metal but with a different atomic weight can be directly used for PET imaging and radiotherapeutic treatments so that the properties of the tracers can be retained. For examples, ^{67}Ga (long half-life = 78 h) is well suited for binding affinity tests *in vitro*, while the corresponding ^{68}Ga can be used for examining biodistribution

Table 1 Half-life and applied method of radionuclides in this review

Radiometal	Half-life ($t_{1/2}$)	Method and emitter used in this review	
^{66}Ga	9.5 h	PET	β^+
^{67}Ga	78 h	SPECT	γ
^{68}Ga	68 min	PET	β^+
^{64}Cu	13 h	PET	β^+
^{67}Cu	62 h	Radionuclide therapy	β^-
^{86}Y	15 h	PET	β^+
^{90}Y	64 h	Radionuclide therapy	β^-
^{111}In	68 h	SPECT	γ
^{177}Lu	161 h	Radionuclide therapy	β^-
^{18}F	110 min	PET	β^+

by PET due to its short half-life (68 min); thus, the patients do not suffer from long periods of radiation exposure.

(3) When suitable radiometal–DOTA–biomolecules have been determined, the tracers are examined for microPET imaging using small animal models, such as rats, implanted with tumor cells. The PET biodistribution data are compared with those obtained by other methods, such as SPECT (γ-scintigraphy imaging) and autoradiography, and the tracers are then evaluated for further optimization. The same DOTA bioconjugate can be used even for MR imaging (magnetic resonance) by incorporating paramagnetic metals, such as Gd^{3+}. Recent trends also utilize DOTA–lanthanide complexes for fluorescence microscopy (either utilizing Tb or Eu) and NIR (near infrared, by metalation with Yb or Er). The principle for these imaging probes is based on the energy transfer from the neighboring chromophores (donors) to the DOTA–lanthanide complexes (acceptors), and has been gradually applied to the current bioimaging purposes.[15,16] Finally, the tracers with good properties can be subjected to clinical applications, namely, PET diagnosis and/or radionuclide therapy for the patients.

The following are recent and representative examples of biomolecule-based PET, mostly directed to cancer diagnosis.

2. Labeling methods of biomolecules with DOTA ligand

Two methods have been widely used for the conjugation of DOTA or its derivatives to peptides, oligonucleotides, antibodies, and proteins (Scheme 1, route 1 and 2). In one method, for the labeling of synthetic peptides, the commercially available tris-*t*-butyl-DOTA[17] is introduced during Fmoc-based solid-phase synthesis [Route 1 (i)]. The *t*-butyl protecting groups of DOTA and other acid-sensitive amino acid side-chain protecting groups are concomitantly removed at the end of peptide synthesis, followed by cleavage of peptides from the resin by treatment with neat TFA (trifluoroacetic acid) or TFA with radical scavengers. However, in some cases, *t*-butyl group deprotection is incomplete, or the DOTA–peptide conjugates decompose under the prolonged acid treatment. Recently, tris-allyl-DOTA was introduced and successfully applied to the DOTA–peptide synthesis.[18] The allyl groups in DOTA were quantitatively removed on the solid phase by treatment with $Pd(PPh_3)_4$–morpholine in dichloromethane, followed by cleavage from the resin to provide the desired DOTA-labeled peptides at a purity sufficient for PET experiments. As a more direct method, DOTA-labeled Fmoc-protected lysine has also been developed [Route 1 (ii)], and applied to the Fmoc-based solid-phase synthesis of DOTA-labeled peptides.[17,19,20]

Secondly, especially for the labeling of proteins or antibodies, DOTA is introduced to the ε-amino group of lysine or the N-terminus of a protein by reaction with DOTA-*O*-succinimidyl ester (DOTA-OSu); the reaction is more favorable with DOTA-*O*-sulfosuccinimidyl ester (DOTA-OSSu), due to the better solubility of this compound in buffer solutions (Route 2). Thus, DOTA-OSSu prepared *in situ* from DOTA, EDC; *N*-(3-dimethylaminopropyl)-*N′*-ethylcarbodiimide, and *N*-hydroxysulfosuccinimide (SNHS), is directly reacted with the biomolecules, usually at room temperature overnight, to give the desired DOTA conjugates. This conventional method, using the activated succinimidyl ester of DOTA, was further improved by optimizing the reaction conditions, both for preparation of the activated DOTA-OSSu and for conjugation. The best conditions for conjugation to biomolecules (in this case, an antibody) involved incubation of the antibody with DOTA-OSSu in 0.1 M sodium phosphate buffer (pH = 7.5) at 4 °C for 24 h. By this method, the number of DOTA molecules introduced to the antibody was increased six-fold, while unfavorable antibody dimerization mediated by the active ester was significantly reduced.[21] This direct labeling method has also been used for conjugation with peptides and oligonucleotides, although the latter requires synthetically introduced amino linkers. The detailed conditions for labeling by DOTA succinimidyl ester, as well as labeling by the other methods that utilize the *p*-nitrophenyl ester or isothiocyanate,[22,23] will be discussed in the following sections.

Although the direct labeling of biomolecules by DOTA (such as using an activated DOTA ester) is quite useful, the reactions usually proceed slowly and require as much as a few milligrams of sample in order to keep reaction concentrations high. Since PET experiments require only small amounts of tracers, and important biomolecules are sometimes obtained in only small amounts, a submicrogram-scale conjugation methodology would greatly expand the applicability towards PET imaging. To address this issue, a submicrogram-scale labeling of lysine residues was developed *via* a rapid 6π-azaelectrocyclization (Route 3).[24] The authors have discovered that unsaturated (*E*)-ester aldehyde derivatives quantitatively react with primary amines, including lysine, within 5 min in solution at a wide range of pH, providing 1,2-dihydropyridines as irreversible products.[25–28] This reaction proceeds *via* smooth aza-electrocyclization of the intermediary Schiff bases (1-azatrienes), which is strongly accelerated due to the efficient HOMO–LUMO interactions within the 1-azatriene systems in the presence of C4-electron withdrawing and C6-conjugated substituents.[26] Not only DOTA, but also other groups used in imaging (such as fluorescent groups), were efficiently and selectively introduced to lysines on a picomole scale, even at 10^{-7}–10^{-8} M concentration of peptides, proteins, and monoclonal antibodies, after an incubation of 5–30 min at room temperature. It is also noteworthy that various metals, such as paramagnetic Gd^{3+}, can be chelated in the DOTA unit of the ester aldehyde probe, prior to the labeling of the peptide (Route 3). Therefore, this new process would allow for the efficient labeling of valuable and/or unstable materials.

3. Peptide-based PET

Cyclic RGD derivatives as $\alpha_V\beta_3$-integrin agonists

α_V-Integrins, cell adhesion molecules that are highly expressed on tumor cells, present attractive targets for tumor imaging. The

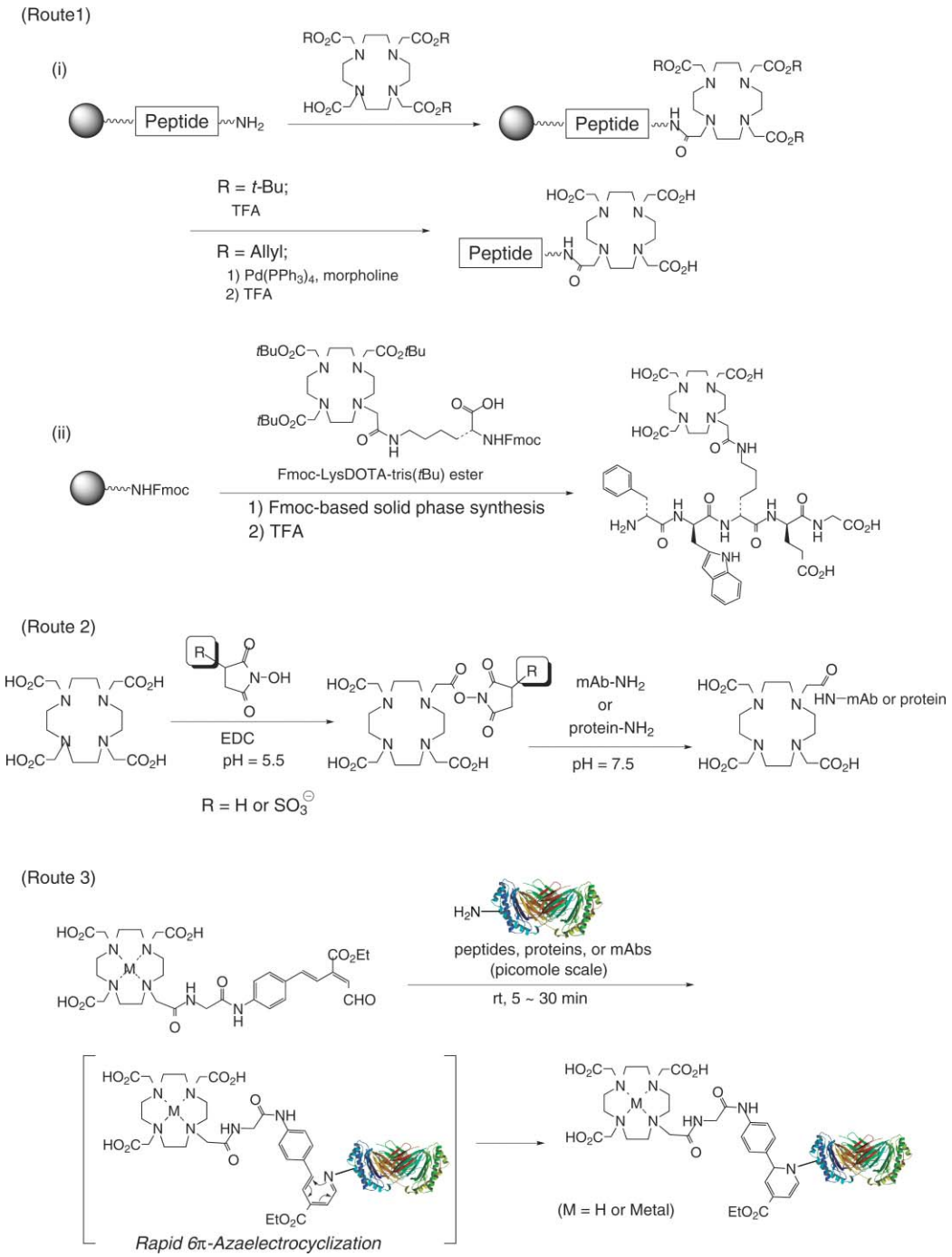

Scheme 1 Conjugation methods with biomolecules.

microPET imaging of a strong $\alpha_v\beta_3$-integrin agonist, c(RGDyK) **1** and its derivatives **2–6** (Fig. 2) have been investigated for breast, brain and lung cancer models. The amino groups of these c(RGDyK) peptides in Fig. 2 were labeled with DOTA with ~60–70% yield, by reaction with DOTA-OSSu, prepared from DOTA, EDC, and *N*-hydroxysulfosuccinimide (SNHS), at 4 °C, pH 8.5 in H_2O overnight. After the introduction of ^{64}Cu, their *in vivo* kinetics and tumor-to-organ ratios were examined based on microPET imaging and whole-body autoradiography. The radiolabeled peptides **1–6** (Fig. 2) were found to accumulate in tumor cells in a receptor-specific manner, since the accumulation was effectively blocked by non-labeled c(RGDyK).

The ^{64}Cu–DOTA conjugate of c(RGDyK) **1** showed prolonged tumor retention in the orthotopic MDA-MB-435 breast cancer model, compared with the [^{18}F]-benzoate derivative (see structure in Fig. 2), which showed fast tumor washout rate and unfavorable hepatobiliary excretion, resulting in significant radioactivity accumulation in the gall bladder and intestines.[29] These results indicate that the overall charge of the molecule introduced by the DOTA moiety has profound effects on tumor accumulation

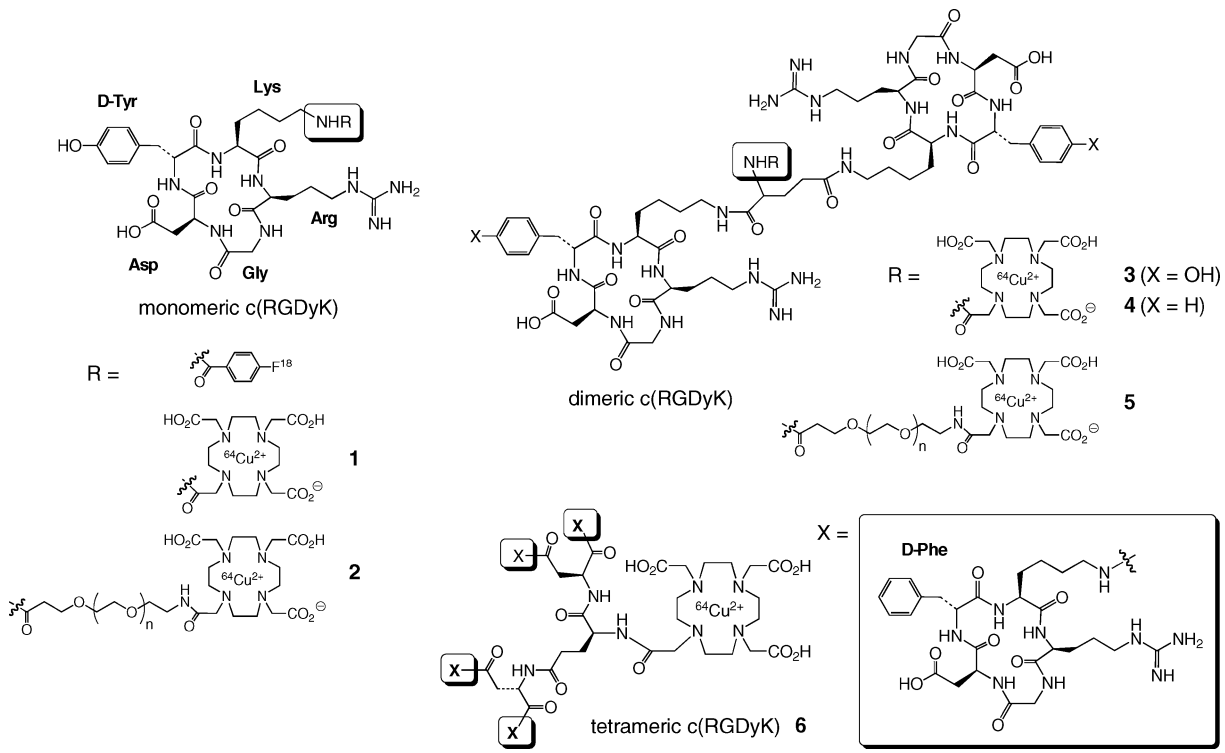

Fig. 2 Cyclic ^{64}Cu-DOTA-RGD derivatives as $\alpha_V\beta_3$-integrin agonists.

and *in vivo* kinetics. In order to further reduce the persistent uptake of **1** in the liver and kidney, the dimeric peptides ^{64}Cu-DOTA-E[c(RGDyK)]$_2$ **3** and ^{64}Cu-DOTA-E[c(RGDfK)]$_2$ **4** were investigated.[30] The dimeric peptide **3** showed high and specific tumor uptake, and better tumor retention than monomeric derivative **1**, presumably due to the bivalency and increase in molecular size. Interestingly, ^{64}Cu-DOTA-E[c(RGDyK)]$_2$ **3** showed better *in vivo* kinetics than the phenylalanine derivative, ^{64}Cu-DOTA-E[c(RGDfK)]$_2$ **4**, presumably due to the increased hydrophilicity.

^{64}Cu-DOTA-PEG-c(RGDyK) **2** was designed to improve the *in vivo* kinetics of **1** by introducing the polyethyleneglycol linker (PEG; MW = 3400) between the peptide and DOTA, and was applied to microPET imaging of both orthotopic and subcutaneous brain tumor models.[31] The properties of PEG derivative **2** were preferable to those of **1**: rapid and high tumor accumulation, rapid blood clearance, significantly reduced liver uptake, and rapid clearance of renal accumulation. Consequently, this tracer achieved high tumor-to-organ ratios. Similarly, the PEG derivative of the dimeric peptide **3**, ^{64}Cu-DOTA-PEG-E[c(RGDyK)]$_2$ **5** showed better properties than dimeric peptide **3**, and was used for lung cancer imaging.[32] The minimum accumulation of non-specific radioactivity in the normal lung tissue and heart led to PET images of high quality for orthotopic lung cancer tumors, both for primary tumors and small metastatic lesions. In contrast, conventional ^{18}F-FDG could only image the primary tumor, whereas metastatic lesions were masked by intense cardiac uptake and high lung background. The only drawback of the two PEG derivatives **2** and **5** is their relatively low receptor binding affinity to $\alpha_V\beta_3$-integrin.

Significantly increased receptor binding affinity, in comparison with monomeric and dimeric peptides **1** and **3**, was realized by tetrameric ^{64}Cu-DOTA-E{E[c(RGDfK)]$_2$}$_2$ **6** by taking advantage of polyvalency effects.[33] Tetrameric peptide **6** also showed excellent *in vivo* properties in female athymic nude mice bearing subcutaneous UG87MG glioma xenografts. Rapid blood clearance and predominant renal excretion, together with the expected rapid and high tumor uptake and slow washout from cancer cells, make the probe a very promising PET tracer for integrin receptor-targeted tumor diagnosis.

Somatostatin derivatives for diagnosis of somatostatin receptor-expressing tumors

Somatostatin-based PET imaging and radiotherapy is of great interest, since somatostatin receptors (SSTRs) are overexpressed in neuroendocrine tumors, *i.e.*, gastroenteropancreatic, small cell lung, breast, and sometimes tumors in the nervous system.[14] Somatostatin is known to be easily degraded *in vivo*, and metabolically stable DOTA–octreotide derivatives have been developed. Out of many analogs prepared so far, [DOTA-D-Phe^1,Tyr^3]-octreotide (DOTA-TOC, **7**, Fig. 3) exhibited the highest affinity to the somatostatin receptor subtype 2 (SSTR2), which can be found in primary tumors as well as metastases; therefore, this probe has been useful for imaging of tumor-bearing mice, non-human primates, and human patients.[34] DOTA-TOC **7**, usually prepared by solid-phase synthesis (Scheme 1, Route 1) was labeled with ^{111}In, ^{90}Y, or ^{67}Ga; binding affinity to SSTR2, internalization/externalization in SSTR2-expressing AR4-2J pancreatic tumor cells, stability in serum, and biodistribution were studied in nude mice implanted with AR4-2J tumor cells.[35,36] ^{67}Ga-DOTA-TOC showed much higher SSTR2 affinity than the corresponding ^{111}In and ^{90}Y congeners and was found to be efficiently internalized by AR4-2J cells. Furthermore, ^{67}Ga-DOTA-TOC was

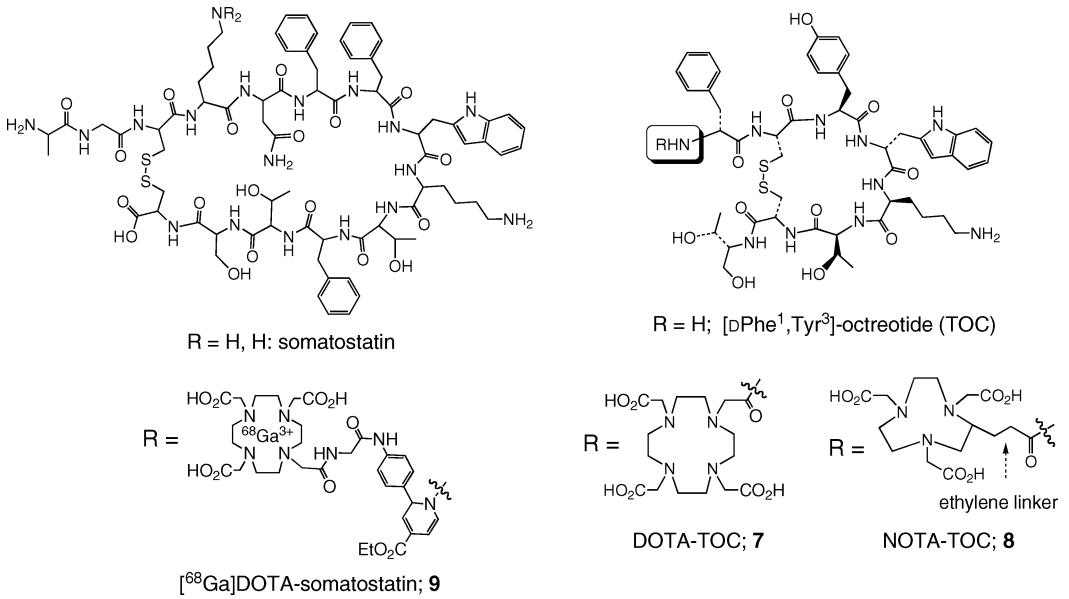

Fig. 3 Somatostatin and octreotide derivatives.

rapidly removed from non-target organs including the kidney, resulting in excellent tumor-to-non-target tissue uptake ratios. The observed metal ion dependence was explained by the differences in the DOTA–metal coordination structures, based on X-ray crystallographic analysis of simplified complex models. Ga^{3+} is hexacoordinated by the four macrocyclic nitrogens and two carboxylates, while one carboxylate group and the amide oxygen are not involved in the metal coordination. This free carboxylate group may contribute to the efficient kidney clearance, while the structure of ^{67}Ga-DOTA-TOC, where the pharmacophoric peptide moiety was sufficiently separated by the free amide linker, resulted in improved receptor binding and hence high tumor uptake.[35,36] On the other hand, the octacoordinated structure of Y^{3+}-DOTA, in which the metal occupies all carboxylates, nitrogens, and amide linker groups, might induce congestion on the probe structure, leading to lower receptor binding affinity.

In order to examine the importance of a chelate–peptide linker for receptor binding, Ga- and In-incorporated NOTA-TOC derivative **8** (Fig. 3), bearing a non-coordinative ethylene spacer and metabolically stable NOTA (1,4,7-triazacyclononane-1,4,7-triacetic acid), was prepared and investigated in the same AR4-2J tumor model.[37] An improved binding affinity to SSTR2 and SSTR5 was observed for both the ^{67}Ga- and ^{111}In-derivatives, thus proving the favorable effects of the non-coordinating ethylene spacer on receptor binding, as well as different metal complex formations with triamine- and tricarboxylic acid-based ligands.

DOTA-TOC **7**, labeled with the positron-emitting radionuclide ^{66}Ga ($t_{1/2} = 9.5$ h) was investigated in AR4-2J-implanted mice by PET,[38,39] and excellent tumor-to-organ ratios could be achieved due to its high receptor affinity. PET imaging of ^{86}Y congener ($t_{1/2} = 15$ h) in non-human primates (baboons, *Papio hamadryas*) has been reported as well.[40] However, these two reports note relatively high uptake in the kidney, which still remains to be improved.

The first PET studies of DOTA-TOC **7** in human patients was reported using ^{68}Ga ($t_{1/2} = 68$ min).[41–45] Meningiomas were selected as the target tumor because SSTR2 is overexpressed in these cancers. ^{68}Ga-DOTA-TOC was injected into patients suffering from meningiomas (tumor size of 7 to 25 mm diameter), and the results were compared with those obtained by SPECT (single-photon emission computerized tomography), MRI (magnetic resonance imaging), as well as ^{18}F-FDG PET. ^{68}Ga-DOTA-TOC was rapidly excreted from the blood, immediately accumulated in the meningiomas after the injection, and even the smallest tumors of 7 to 8 mm diameter could be clearly visualized. The ^{68}Ga-DOTA-TOC tracer also detected the extent of meningiomas located beneath osseous structures, such as at the base of the skull. It is worthwhile mentioning that no radioactivity could be observed in normal brain tissues. On the other hand, SPECT and MRI have a sensitivity drawback in detecting small meningiomas, *i.e.*, the methods failed in visualizing tumors at the base of the skull. Furthermore, the use of the conventional ^{18}F-FDG PET tracer resulted in lower meningioma-to-background ratios. Therefore, the ^{68}Ga-DOTA-TOC probe is a very promising candidate not only as a PET tracer of SSTR-positive tumors but also for radiotherapeutic applications, when suitable radiometals, such as ^{67}Ga, ^{90}Y, or even ^{67}Cu are used. DOTA-TOC **7** could be applied not only to PET, but also to diagnosis by SPECT of patients with differentiated thyroid cancer (DTC), which is difficult to accomplish by conventional measurements of serum thyroglobulin (Tg) levels and ^{131}I whole-body scintigraphy (^{131}I-WBS).[46]

Finally, in order to circumvent the unfavorable kidney accumulation of the radiometal-DOTA-TOC tracer **7** during clinical treatments, amino acid co-infusion has been examined.[47,48] ^{86}Y-DOTA-TOC was administered to 24 patients with metastatic, non-resectable, neuroendocrine tumors, and the effects of co-infusion were monitored by PET. Renal uptake of ^{86}Y-DOTA-TOC could be reduced by infusion of a mixture of L-lysine and L-arginine, and more efficiently by the dipeptide Lys-Arg, without affecting tumor uptake. Although such a co-infusion of amino acids allows the patients to receive a higher dose of the tracers to be accumulated

in the target tumors, the side effects of nausea and vomiting should be taken into consideration.

As described above, somatostatin itself was believed to be extremely unstable *in vivo* (stability in rat serum for just 5 min), and the previous imaging studies of somatostatin receptors were in all cases effected using metabolically stable octreotide analogs. However, a recent study on microPET imaging of ^{68}Ga-DOTA-somatostatin **9** (Fig. 3), prepared by selective labeling of a single lysine that is not responsible for receptor binding (Scheme 1, Route 3), successfully visualized the tracer accumulated in the pancreas of rabbit 2–4 h after injection (Fig. 4).[24] Given this new evidence of somatostatin stability in rabbit, as well as its clear accumulation in the pancreas (somatostatin receptors are expressed on the pancreas and kidney, as well as the gastrointestinal tract),[14] this study might provide an intriguing opportunity to use somatostatin itself as a diagnostic tracer of endocrine tumors.

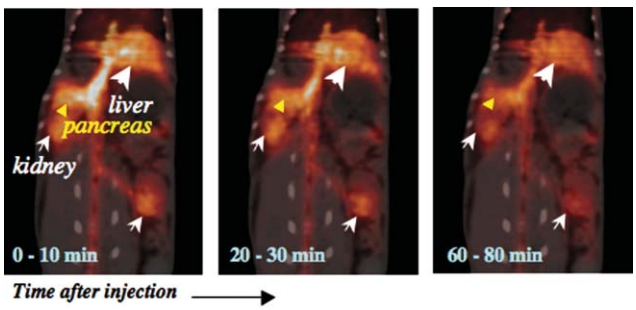

Fig. 4 PET imaging of ^{68}Ga-DOTA-somatostatin **9** in rabbit (axial view, overlapped with CT). The images represent time-dependent changes of accumulation in liver (large arrow), kidney (small arrow) and pancreas (arrowhead) after injection of ^{68}Ga-DOTA-somatostatin.

Bombesin derivatives for imaging of human prostate cancer

Bombesin, a peptide of 14 amino acids, shows high affinity to the human gastrin-releasing peptide receptor (GRPR), which is overexpressed on cancer tissues such as breast, gastrointestinal, prostate, and small cell lung cancers. ^{64}Cu-DOTA-[Lys^3]bombesin **10** (Fig. 5) has been extensively investigated for imaging of the overexpression of GRPR in both androgen-dependent and androgen-independent human neoplastic prostate tissues.[49] The lysine ε-amino group in [Lys^3]bombesin was labeled with DOTA in 75% yield, by reaction with DOTA-OSSu at 4 °C, pH 8.5–9.0 in H_2O overnight. The biodistribution, whole-body autoradiographic imaging, and microPET of **10** in PC-3 (androgen-independent) and CWR22 (androgen-dependent) prostate cancer tumor models achieved strong tumor-to-background contrast for both cancer models, although the radiotracer uptake was higher in the androgen-independent PC-3 tumor than the androgen-dependent CWR22 tumor. A receptor blocking study using co-injection with cold [Lys^3]bombesin concluded that the radioactivity accumulation in the PC-3 tumor was receptor-specific, whereas the accumulation in CWR22 tumor was attributed to non-specific uptake.

A truncated bombesin(7–14) analog of **10**, ^{64}Cu-DOTA-Aca-bombesin(7–14) **11** (Aca: ε-aminocaproic acid) has also been studied in the same human prostate adenocarcinoma models. This analog was found to be unstable—**11** decomposed 30 min after the injection—as also supported by the stability studies in

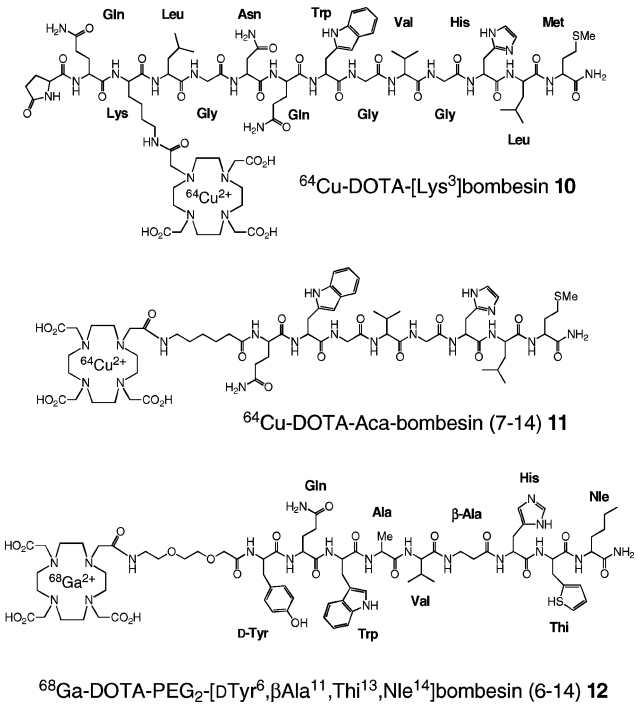

Fig. 5 ^{64}Cu- and ^{68}Ga-DOTA-bombesin derivatives.

blood, urine, tumor, liver, and kidney by HPLC.[50,51] Taking into consideration that **10** shows higher GRPR affinity than **11** (IC_{50} = 18.4 ± 0.2 nM for **11** and 2.2 ± 0.5 nM for **10**), ^{64}Cu-DOTA-[Lys^3]bombesin **10** has a greater potential for clinical applications.

On the other hand, another truncated analog, ^{68}Ga-DOTA-bombesin(6–14) **12** showed high affinity to the GRPR receptor as well as rapid internalization and dose-dependent uptake in AR4-2J tumor cells.[52] Furthermore, a prolonged tumor residence time and rapid clearance from GRPR-negative tissues in AR4-2J tumor-implanted mice (pancreas carcinoma xenograft), resulted in favorable tumor-to-organ ratios as early as 1 h after the injection; the results make this tracer a promising candidate for diagnostic applications.

α-Melanocyte stimulating hormone (α-MSH) analogs for detection of malignant melanoma

Since the receptor of α-melanocyte stimulating hormone (melanocortin type 1 receptor; MC1R) is overexpressed in both melanotic and amelanotic melanoma tissues, sensitive and high resolution PET imaging with α-MSH-based tracers (Fig. 6) has great potential for early detection of malignant melanoma. This is especially important because the prognosis of patients with metastatic melanoma is currently very poor. Furthermore, ^{18}F-FDG is a notoriously inaccurate tracer, particularly for detection of small foci, due to its significant background signals.

DOTA-[Lys^{11}]NAPamide **13** (NAPamide: [Nle^4,Asp^5,D-Phe^7]-α-MSH(4–11)) was synthesized in 15% overall yield from the NAPamide peptide, by the reaction of the Lys^{11} ε-amino group with tris-*t*-Bu-DOTA in the presence of HATU; 1-[bis(dimethylamino)methylene]-1*H*-1,2,3-triazolo(4,5-*b*)pyridinium 3-oxide hexafluorophosphate, *N*,*N*′-diisopropylethylamine in DMF, followed by the deprotection of *t*-butyl groups with TFA.[53] After the incorporation of ^{111}In, ^{67}Ga, or ^{68}Ga as a short-lived

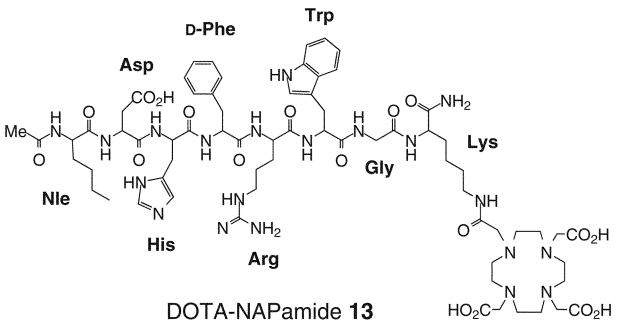

DOTA-NAPamide **13**

[Nle^4,Asp^5,D-Phe^7,DOTA-Lys^{11}]-α-MSH (4-11)

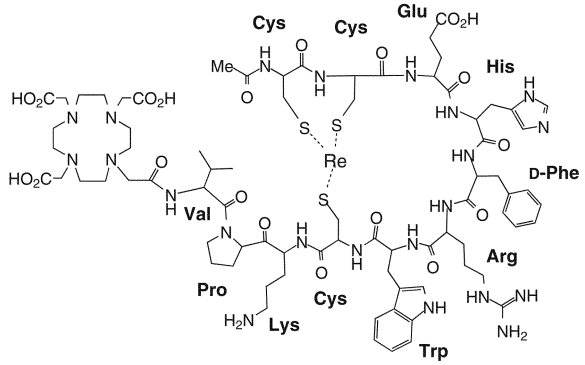

DOTA-ReCCMSH (Arg^{11}) **14**

DOTA-Re-[Cys^{3,4,10},D-Phe^7]-α-MSH (3-13)

Fig. 6 DOTA-α-melanocyte stimulating hormone (α-MSH) derivatives.

positron emitter for PET, the compound's *in vivo* properties were evaluated in the mouse tumor model implanted with B16/F1 murine melanoma. Both ^{111}In-DOTA- and ^{67}Ga-DOTA-[Lys^{11}]NAPamides showed high tumor and low kidney uptakes resulting in excellent tumor-to-kidney ratios. The uptake of ^{67}Ga-DOTA-[Lys^{11}]NAPamide in the liver could be further reduced by co-infusion of L-lysine, without affecting tumor uptake. The autoradiographs of the ^{67}Ga congener successfully detected the primary melanoma in the skin, as well as metastatic melanoma in the lung and liver. The microPET also visualized the high and selective tumor uptake that makes the ^{68}Ga-DOTA-[Lys^{11}]NAPamide tracer a promising tracer for melanoma diagnosis.

MicroPET imaging of ^{64}Cu or ^{86}Y congeners of DOTA-ReCCMSH(Arg^{11}) (**14**, Re = rhenium), another cyclic analog of α-MSH, has also been studied in mice bearing B16/F1 murine melanoma tumors.[54,55] The microPET visualized the tumor within 30 min after the injection, in good agreement with the biodistribution data obtained by the other methods. The profound effects of radiometals on the *in vivo* kinetics, similar to those observed in the case of octreotides (see above), can also be seen here; non-target organ uptake was considerably lower for the ^{86}Y congener, except in the kidney.

Human epidermal growth factor (hEGF) for diagnosis of malignant tumors

Overexpression of epidermal growth factor receptor (EGFR) in many carcinomas provides a unique opportunity to apply EGF derivatives as peptide-based PET tracers. DOTA-hEGF (human epidermal growth factor), as a mixture of mono-, bis-, and tri-DOTA derivatives, was prepared by the treatment of hEGF with DOTA-OSu at pH 9.0 in borate buffer at room temperature overnight.[56] High affinity for the EGFR, receptor-specific uptake, rapid internalization, and good retention of the radioactivity in tumor cells were observed when the ^{64}Cu congener was investigated *in vitro* with U343 glioma cells and A431 cervical carcinoma cells; these were chosen because both cell lines overexpress EGFR. MicroPET of the same tracer, namely, ^{64}Cu-DOTA-hEGF in BALB/c *nu/nu* mice implanted with A431 carcinoma xenografts, quickly visualized the radioactivity accumulation both in xenografts and in EGFR-expressing organs.

4. Antibody-based PET diagnosis

The specific localization of radiometal-labeled antibodies to target tumors is a promising approach for PET diagnosis.[57] However, the use of whole antibodies suffers from their unfavorable properties *in vivo*, such as prolonged biological half-lives and slow blood clearance, which result in low tumor-to-background ratios. On the other hand, the enzymatically generated antibody fragments, such as F(ab′)$_2$ or Fab′ (termed "minibodies"), show more favorable tumor targeting and clearance kinetics than the corresponding whole antibodies. In this section, a few prominent examples of minibody-based PET will be described. Furthermore, the concept of "pretargeted" immunodiagnosis using a whole antibody will also be discussed.

Anti-HER2 protein antibody, herceptin

HER-2 (c-erbB2 or Her-2/neu) is a protooncogene, which encodes the 185-kDa transmembrane protein, human epidermal growth factor receptor 2 (HER2 protein). HER2 protein is overexpressed particularly in primary breast cancers as well as in other malignancies, whereas it is expressed at low levels in normal tissues. Therefore, herceptin (trastuzumab), a clinically applied anti-HER2 protein antibody, is a very attractive PET tracer for tumor imaging. Although herceptin itself shows good *in vivo* distribution and pharmacokinetics for PET study, the frequent injection of the whole antibody is not possible due to its long half-life, especially in clinical applications in live human patients. On the other hand, the F(ab′)$_2$ fragment of herceptin has a much shorter half-life, and is therefore suited for diagnostic purposes.[58]

The F(ab′)$_2$ fragment of herceptin, which was obtained by pepsin digestion of herceptin, was conjugated with DOTA by treatment with DOTA-OSu at pH 7.3 in water.[59,60] Characterization of the biodistribution, including microPET studies, were performed in mice bearing BT474 breast tumor xenografts, by using the ^{111}In and ^{68}Ga congeners, respectively. ^{111}In-DOTA-F(ab′)$_2$-herceptin significantly accumulated in the HER2-overexpressed BT474 xenograft, whereas little accumulation was observed in MDA-MB-468 xenografts with high levels of EGFR (epidermal growth factor receptor) expression; thus, the tracer achieved good tumor selectivity. Subsequently, microPET of ^{68}Ga-DOTA-F(ab′)$_2$-herceptin in a mouse cancer model was also examined in response to treatment with a Hsp-90 inhibitor, 17-allylamino-17-demethoxygeldanamycin (17AAG). Hsp90 (heat shock protein 90) is a molecular chaperone which plays important roles in the folding

and stabilizing of oncoproteins; PET of ^{68}Ga-DOTA-F(ab′)$_2$-herceptin could follow the tumor expression and reduction, thus evaluating the drug pharmacodynamics of 17AAG. A significant decrease in HER2 protein was successfully visualized by this ^{68}Ga tracer after treatment with 17AAG. In contrast, PET signals from the conventional ^{18}F-FDG tracer, which only measures the glycolysis inside the cells (an independent consequence of the HER2 downregulation), were unchanged.

Anti-carcinoembryonic antigen (CEA) antibody, cT84.66

MicroPET imaging of the truncated fragment of anti-carcinoembryonic antigen (CEA) antibody, cT84.66, was investigated in athymic mice bearing paired xenografts LS174T human colon carcinoma (CEA positive), and C6 rat glioma (CEA negative). An scFv-C_H3 fragment of cT84.66 was used (Fig. 7), taking advantage of the rapid accumulation and high retention of the minibody in the tumor tissue, together with its rapid blood clearance.[61] The scFv-C_H3 minibody was conjugated with DOTA by reaction with DOTA-OSSu at 4 °C for 18–24 h in water under neutral conditions (minibody : DOTA ratios = 1 : 5–1 : 6).[62] MicroPET images of the ^{64}Cu-labeled minibody detected much higher uptake in CEA-positive LS174T human colon carcinoma than in CEA negative C6 rat glioma tumor. Low uptake was observed in most other organs except in the liver, making this engineered minibody a new class of the "minibody"-based PET tracer of tumors.

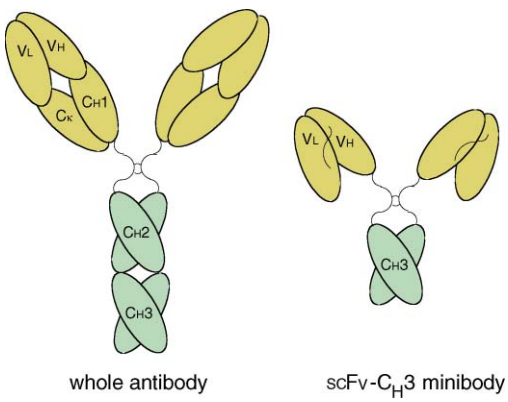

Fig. 7 Anti-CEA antibody, cT84.66 and truncated minibody.

Although PET imaging of whole anti-CEA antibody (cT84.66) has not been performed, an efficient DOTA conjugation method to this antibody has been reported, as described in section 2.[21]

Anti-cell adhesion molecule (CAM) antibodies

Cell adhesion molecules (CAM) are usually highly expressed in cancer cells. For example, L1 cell adhesion molecule (L1-CAM) is overexpressed in renal, ovarian, and endometrial carcinomas. Therefore, anti-L1-CAM antibody-based imaging, directed towards radioimmunotherapy (RIT), has been investigated in nude mice bearing SK-N-BE2c xenografts. The divalent chCE7F(ab′)$_2$, a truncated fragment of a whole anti-L1-CAM antibody (chCE7a), shows improved clearance and *in vivo* biodistribution properties.[63] The truncated form was efficiently prepared in HEK-293 cells and conjugated with two different kinds of DOTA derivatives, NCS-DOTA **15** and tri-glycyl NCS-DOTA **16** (Fig. 8) by reaction in 0.1 M sodium phosphate buffer (pH = 9–10) at 4 °C for 16 h (DOTA : minibody ratios = *ca.* 2 : 1, NCS = isothiocyanate). A tri-glycyl linker was introduced in order to prevent unfavorable kidney accumulation of the radiometal-labeled metabolites, often observed following minibody degradation in serum. After labeling with ^{64}Cu as a positron emitter for PET and ^{177}Lu and ^{67}Cu as β$^-$ emitters for other biodistribution studies as well as for radioimmunotherapeutic purposes, the kinetics of uptake in tumor xenografts were evaluated in mice. NanoPET successfully visualized efficient accumulation in xenografts and peritoneal metastases, which is in good agreement with results obtained in other biodistribution studies. These studies concluded that among the tracers studied, $^{64/67}$Cu-triglycyl-DOTA-chCE7F(ab′)$_2$ is superior for both PET and radioimmunotherapy due to the favorable tumor-to-organ ratios, especially the tumor-to-kidney ratio. Nevertheless, these $^{64/67}$Cu-based tracers still exhibit high kidney uptake, which remains to be improved for further applications in patients.

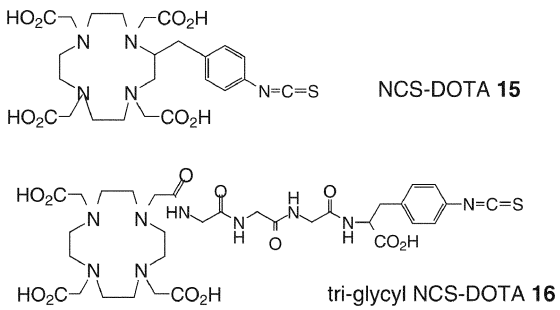

Fig. 8 Reactive DOTA-NCS (isothiocyanate) reagents.

A very interesting "pretargeted" PET strategy using an anti-Ep-CAM antibody (NR-LU-10) (Fig. 9) was reported in a xenograft-implanted mouse model of the human colorectal cancer, SW1222.[64] For this protocol, the monoclonal antibody NR-LU-10 was first conjugated with streptavidin and injected into the xenograft-bearing mouse, prior to treatment with ^{64}Cu-DOTA-biotin **17** (thereby called a "pretargeted" strategy). The stability, clearance, biodistribution, and tumor targeting properties of

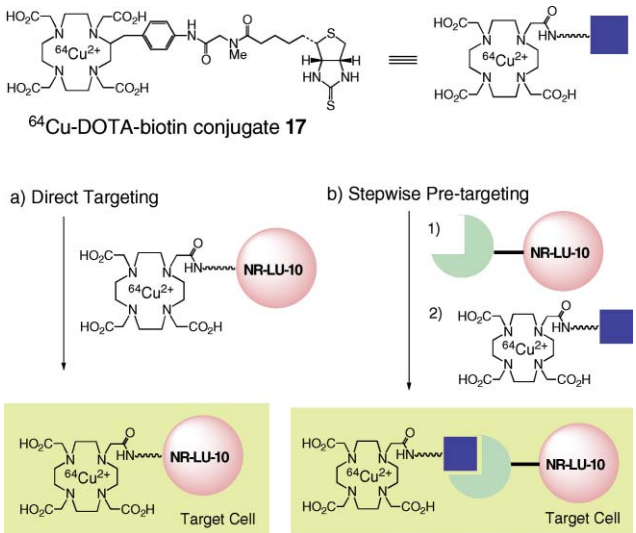

Fig. 9 "Pretargeted" strategy of PET diagnosis.

^{64}Cu-DOTA-biotin **17** in the "pretargeted" xenograft have been compared with those of the conventional antibody-based PET targeting by ^{64}Cu-DOTA-NR-LU-10, which is prepared *via* direct labeling of the antibody with DOTA-OSSu. As expected, the small effector molecule of ^{64}Cu-DOTA-biotin **17** exhibited more rapid tumor uptake, substantially faster blood clearance and renal excretion, therefore resulting in superior tumor-to-normal tissue ratios. "Pretargeted" PET is thus a new and promising strategy for future antibody-based diagnosis.[65,66]

Anti-CD90.2 (Thy1.2) antibody for tumor-specific T-cell trafficking behavior

It is of great clinical interest to image the trafficking behavior of tumor-specific CD^{8+} T-cells by PET. Mice (BALB/c-Thy1.1) bearing the CMS5 tumor were treated with *in vitro*-stimulated DUC18 T-cells, and their distribution was investigated by a T-cell specific antibody tracer.[67] Anti-CD90.2 (Thy1.2) antibody was used for this purpose, and the antibody was labeled with ^{64}Cu-DOTA *via* the DOTA-OSSu method. MicroPET visualized the DUC18 T-cells as they were transferred to all the major secondary lymphoid organs, including small lymph nodes, as well as to tumors. Thus, tumor-specific T-cells do not preferentially accumulate in tumors, but they also stay in the lymphoid organs; this lymphoid localization did not change during or after elimination of the tumors.

5. Miscellaneous (albumins, oligonucleotides, and oligosaccharides)

Serum albumins as PET blood-pool markers

Since the growth of tumors depends on sufficient blood supply, radiolabeled serum albumins are useful for blood-pool imaging of angiogenic tumors, as well as for myocardial perfusion imaging. ^{124}I-labeled albumin might be a candidate for this strategy, but its long half-life ($t_{1/2}$ = 101 h) exposes the patients and their environment to radiation for an unacceptably long time. The ^{68}Ga–DOTA conjugate of rat serum albumin (RSA) as an alternative PET blood-pool marker, *i.e.*, a tracer of blood volume, has therefore been investigated in male ACI rats bearing the subcutaneous Morris heptama, MH3924A.[68] Prior to application to blood-pool imaging, labeling conditions have been thoroughly examined by using a variety of DOTA active esters (Fig. 10).[69] The labeling was efficiently performed by reaction with the 4-nitrophenyl ester of DOTA in 0.1 M phosphate buffer (pH = 8.0) at room temperature overnight, resulting in two DOTA molecules attached per RSA. It is important to limit the number of labeling molecules to two, in order to prevent the sequestration of the modified RSA in tumor cells by the monocyte/phagocyte system. The time-dependent biodistribution study of ^{67}Ga-DOTA-RSA in a xenograft-bearing rat, used as a clinically applicable ^{68}Ga congener, showed slow plasma clearance and good metabolic stability *in vivo*. The HPLC analysis detected a single metabolite in urine, ^{67}Ga-DOTA, likely formed by enzymatic amide hydrolysis. Successful microPET images of the small blood pool around the tumors, as well as the favorable biokinetics, indicate that the compound is well suited for use as a new PET blood-pool tracer. These findings will be further extended to clinical applications by use of ^{68}Ga-DOTA-human serum albumin (HSA).

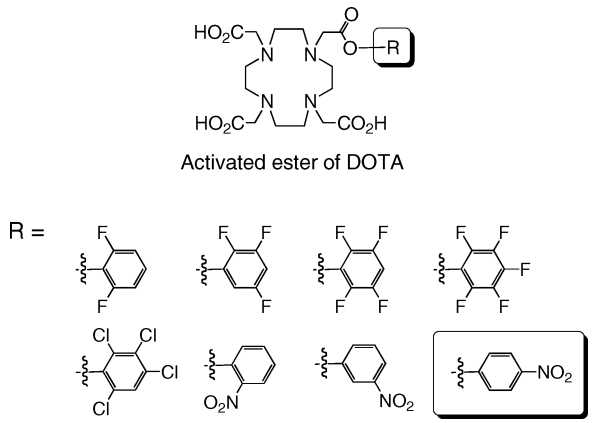

Fig. 10 Reactive DOTA reagents with various electron-deficient phenyl esters.

The PET-based blood-pool method described above, using ^{68}Ga-DOTA-albumins, has been applied to the mechanistic investigation of the inhibition of malignant tumor growth by human angiotensin (hANG).[70] hANG is one of the most potent inhibitors of endothelial cell proliferation, angiogenesis, and tumor growth *in vivo*. Changes in tumor perfusion and blood volume during the angiogenic process in the presence of overexpressed hANG were evaluated by PET, in ACI or RNU nude rats bearing subcutaneous MH3924A. While ^{68}Ga-DOTA-albumin was applied as a blood-volume tracer in the intravascular space of the tumor tissues, $H_2{}^{15}O$ was also used as an inert and freely diffusible tracer for tissue perfusion. MicroPET of these tracers showed that tumor perfusion and blood volume was enhanced in hANG-overexpressed MH3924A compared with the wild-type MH3924A tumor, corresponding to both increased microvessel density and decreased necrosis. It is hypothesized that the improvement of perfusion in response to hANG treatment might correlate with the decrease in interstitial fluid pressure and the normalization of tumor vasculature, leading to diminished hypoxia, *i.e.*, the more efficient exchange of oxygen and nutrients as well as an improved removal of toxic metabolites from tumor tissues.

In a similar way, the tumor inhibition process by human tropinin I (TnI), another potent inhibitor of angiogenesis, was also studied in the same ACI nude mice, this time bearing MH3924A overexpressing TnI.[71] In contrast to the hANG case, decreased tumor perfusion and vascularization were observed, but blood volume was unchanged, presumably due to a different mechanism of angiogenesis inhibition. Thus, ^{68}Ga-DOTA-albumin can be used as a sensitive PET tracer for characterizing the angiogenesis process in response to inhibitors.

Oligonucleotides and peptide nucleic acids (PNA) for tumor imaging

Antisense-based cancer PET imaging is a newly emerging area of non-invasive diagnosis technique. Since ras oncogene point mutations are found in a variety of human tumors but not in normal tissues (*e.g.*, they are expressed in an extremely high ratio in pancreatic carcinomas), the ras messenger RNA (mRNA) is an attractive target for gene-based diagnosis. 17-Mer oligonucleotides consisting of a base sequence of 5′-CTACGC-CACTAGCTCCA-3′ with three metabolically stable backbones,

namely, 2′-deoxyphosphodiester (PO, **18**), 2′-deoxyphosphorothioate (PS, **19**), and 2′-*O*-methyl phosphodiester (OMe, **20**) have been designed to target the codon 12 point mutation of human K-ras oncogene (Fig. 11).[72,73] After labeling by ^{64}Cu-DOTA at the 5′-aminohexyl moiety of the oligonucleotides *via* the DOTA-OSSu method, their biokinetics, biodistribution, and microPET were examined in athymic rats, bearing either a tumor of A549 cells with K-ras point mutation in codon 12, or a tumor of BxPC-3 cells with wild-type K-rasA.[74]

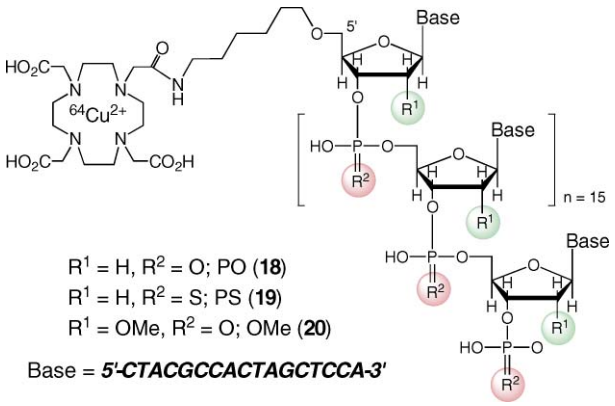

Fig. 11 ^{64}Cu-DOTA-oligonucleotide-based PET tracers.

Better localization images were obtained from microPET of A549 cells when using PS **19** and OMe **20** than when using PO **18**, while a slightly better uptake of PS **19** was observed in A549 cells than in BxPC-3 cells with wild-type K-rasA. However, the nuclease-mediated rapid degradation of OMe **20** and the low tumor selectivity, as well as non-specific accumulation of PS **19** in the kidney, require further improvements of these tracers: metabolic stability, hybridization ability, cell permeability, and binding specificity must all be addressed. In addition, the effects of the oligonucleotide length on biodistribution should be investigated in detail for future applications.

In order to circumvent the metabolic instability of the oligonucleotides, the application of peptide nucleic acid (PNA) congeners to gene-based PET have also been reported.[75] PNA is resistant to endo- and exonuclease degradation, and is known to exhibit high and specific binding to complementary DNA and RNA. The fact that PNA does not activate RNAse H for degradation of the target mRNA also makes PNA tracers a promising candidate. The antisense hybrid PNA, DOTA-Y-PNA50-K4 **21** (Fig. 12) was synthesized for targeting the *unr* mRNA that is highly expressed in a breast cancer cell line (MCF-7). This tracer has the sequence TGGTGTGCTTTGTGGATG, complementary to the *unr* mRNA, and four lysines at the C-terminus to allow for cell permeation.

A biodistribution study showed low uptake and efficient clearance of the ^{64}Cu congener in blood and muscle, but high uptake and long retention in the kidney, when administered intravenously or intraperitoneally in normal BALB/c mice. MicroPET in CB-17SCID mice implanted with MCF-7 tumors showed reproducible tumor-to-muscle ratios, thus achieving the best tumor imaging quality among the oligonucleotide-based PET tracers so far reported. Nonetheless, the tumor-to-muscle ratio of ^{64}Cu-**21** was only four times higher than that of the corresponding sense PNA

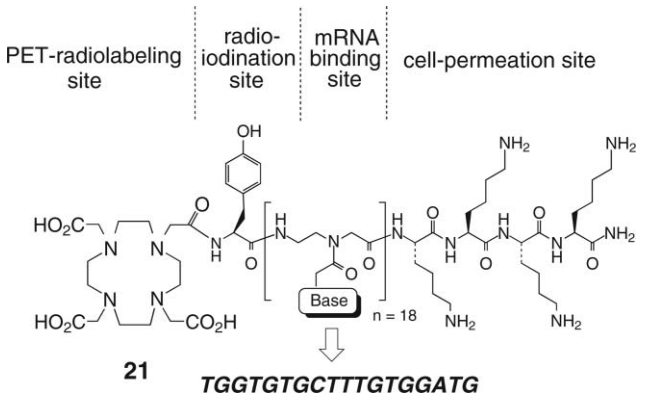

Fig. 12 ^{64}Cu-DOTA-PNA-based PET tracer.

tracer used as a control; therefore, further improvements of the PNA-based tracers are still required.

Visualization of sialic acid-dependent circulatory residence of glycoproteins by PET

Although FDG is widely used as a monosaccharide PET tracer for cancer diagnosis, PET of oligosaccharides and glycoproteins is a totally unexplored field. Very recently, the first microPET of the glycoproteins orosomucoid and asialoorosomucoid was reported in order to investigate the effects of *N*- and/or *O*-glycans on the metabolic stability of the proteins.[24] Based on the smooth electrocyclization protocol (Scheme 1, Route 3), glycoproteins available in only small amounts (62 μg of orosomucoid and asialoorosomucoid) were labeled successfully with the incorporation of ~2–3 units of DOTA by incubating the respective protein with 10 equivalents of aldehyde probe **22** for 30 min, followed by purification by quick size-partitioning gel-filtration (Scheme 2). The DOTA-labeled glycoproteins were subsequently

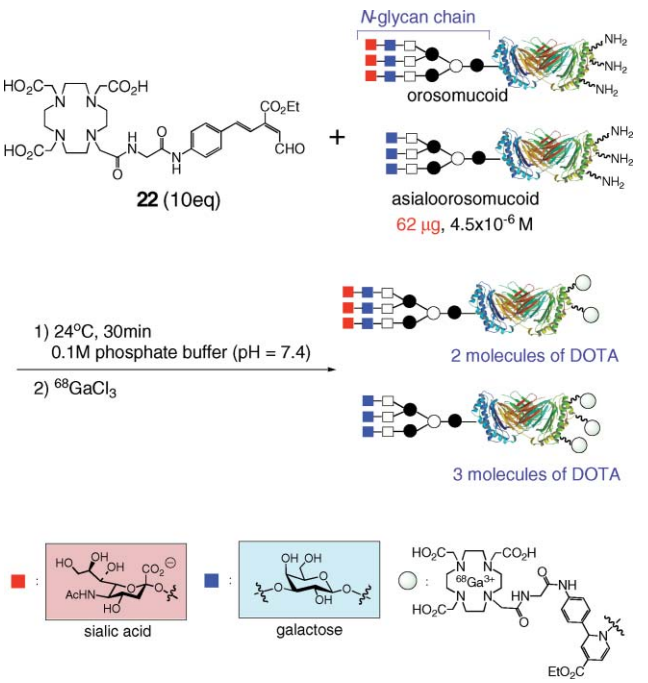

Scheme 2 Labeling of glycoproteins by DOTA.

radiometalated with ^{68}Ga and their *in vivo* kinetics were analyzed in rabbit by means of PET. ^{68}Ga-DOTA-orosomucoid and asialoorosomucoid adducts successfully visualized the asialoglycoprotein being cleared through the kidney faster than the orosomucoid (Fig. 13), thus achieving the first imaging of sialic acid-dependent circulatory residence of glycoproteins. The results are in good agreement with well-known hypotheses of the clearance of the proteins through the asialoglycoprotein receptor in the liver:[76] namely, the sialic acid residue on the non-reducing end of the oligosaccharides contributes to the stability of glycoproteins in the blood, while the sialidase-mediated production of asialoglycoproteins, bearing the galactose residue at the non-reducing end of the oligosaccharides, is responsible for the metabolic pathway. These promising PET images of glycoproteins suggest future uses for the glycoproteins in pharmacological and/or clinical applications.

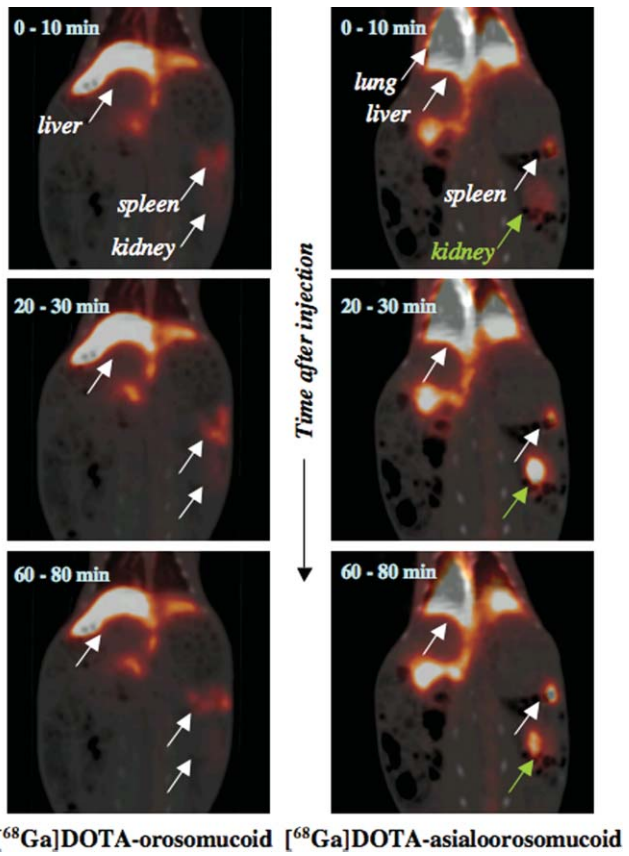

Fig. 13 Dynamic microPET images of ^{68}Ga-DOTA-glycoproteins in rabbits. Time course of accumulation of ^{68}Ga-DOTA-orosomucoid (left) and ^{68}Ga-DOTA-asialoorosomucoid (right) in some peripheral organs (axial views). These PET images were fused to anatomical images obtained by using CT.

6. Future perspective

As is clear from the selected examples cited in this review, PET imaging of biomolecules has recently become one of the most promising strategies for tumor diagnosis, due to the close collaboration between chemists, biologists, and physicians. Specifically, the chemists efficiently synthesize the peptides or the oligonucleotide sequences, and label them with the radiometal-DOTA complexes, while the molecular biologists provide the monoclonal antibodies (or preferably the engineered minibodies). These candidates are first examined *in vitro*; binding affinity to the target receptors, cell internalization, and retention in the tumor cells are all characterized at this stage. The biologists and physicians then characterize the compounds' biodistribution in search for the most favorable kinetics, such as tumor uptake, blood clearance, or tumor-to-organ ratios; at this stage, researchers use small animal models and make measurements on the basis of SPECT, autoradiography, and microPET. The data obtained here feed back to the chemists and the biologists who then strive to improve the tracers, which will ultimately be used for clinical applications.

From a chemistry point of view, if the labeled biomolecules could be more easily accessed, one could more rapidly discover favorable PET tracers, thus greatly expanding the biomolecule-based PET strategy. Although PET experiments require only a few nanograms to micrograms of the tracers, under the current labeling protocols, as much as 5–20 mg of the engineered mAbs must be used. Once more rapid and efficient labeling chemistry is developed, we can find a new way to utilize unstable, important, and precious materials for diagnosis. Once promising candidates for peptide- or oligosaccharide-based tracers are determined, modular approaches to the chemistry will facilitate the optimization of the best tracer from combinatorial libraries. We will then be able to use PET not only for diagnosis and clinical applications but also for elucidating a new signaling pathway stemming from the selected tracers; hence, the development of such bioconjugate chemistry is necessary.

The investigation of dual detection probes, *e.g.*, probes that are detectable both by PET and fluorescence, will also become more important. A new molecular imaging probe has now been developed by taking advantage of the unique energy transfer of the lanthanide–DOTA complexes, which has led to the emerging field of fluorescence techniques. Such a new design of the probes will greatly facilitate biomolecule-based PET, where the stability of the tracers can be simultaneously detected by HPLC.

Following peptides, antibodies, proteins and oligonucleotides as mainly described in this review, the authors strongly believe that oligosaccharide-based tracers are the next candidates to be developed. Surprisingly, to the best of our knowledge, oligosaccharide-based PET has not been reported, except in the case of the ^{18}F-FDG tracer (technically a monosaccharide) and very limited examples of glycoproteins. This is due to the difficulty in obtaining structurally pure oligosaccharides from nature, and also because synthetic methods for complex oligosaccharides still have not been fully established. In addition, the biological activity of oligosaccharides is closely related to their heterogeneous environment, *i.e.*, on the proteins (*O*- or *N*-linked glycans) and on the cell surfaces (such as ceramides), which are usually composed of clusters of mixed oligosaccharides. When such complex and structurally pure oligosaccharide molecules are easily accessible by chemical synthesis, and when the heterogeneous environment of oligosaccharides can be mimicked, it may be possible to target either tumors or inflammation more efficiently than by peptide- or antibody-based tracers.

Acknowledgements

We acknowledge Professor Yasuyoshi Watanabe and Dr Hiroshi Mizuma at RIKEN, Japan for helpful discussion in preparing the manuscript. Parts of the work cited in this review were financially supported by Grants-in-Aid for Scientific Research No. 19681024 and 19651095 from the Japan Society for the Promotion of Science, Collaborative Development of Innovative Seeds from Japan Science and Technology Agency (JST), New Energy and Industrial Technology Development Organization (NEDO, project ID: 07A01014a), research grants from Yamada Science Foundation, as well as the Molecular Imaging Research Program, Grants-in-Aid for Scientific Research from Ministry of Education, Culture, Sports, Science and Technology (MEXT).

References

1 S. S. Gambhir, *Nat. Rev. Cancer*, 2002, **2**, 683–693.
2 M. Suzuki, H. Doi, M. Bjorkman, Y. Anderson, B. Langstrom, Y. Watanabe and R. Noyori, *Chem.–Eur. J.*, 1997, **3**, 2039–2042.
3 M. Suzuki, R. Noyori, B. Langstom and Y. Watanabe, *Bull. Chem. Soc. Jpn.*, 2000, **73**, 1053–1070.
4 M. Suzuki, H. Doi, T. Hosoya, B. Langstrom and Y. Watanabe, *Trends Anal. Chem.*, 2004, **23**, 595–607.
5 T. Hosoya, K. Sumi, H. Doi, M. Wakao and M. Suzuki, *Org. Biomol. Chem.*, 2006, **4**, 410–415.
6 M. F. Loncin, J. F. Desreux and E. Merciny, *Inorg. Chem.*, 1986, **25**, 2646–2648.
7 W. P. Cacheris, S. K. Nickle and A. D. Sherry, *Inorg. Chem.*, 1987, **26**, 958–960.
8 K. Kumar, M. Magerstadt and O. A. Gansow, *J. Chem. Soc., Chem. Commun.*, 1989, 145–146.
9 C. J. Broan, J. P. L. Cox, A. S. Craig, R. Kataky, D. Parker, A. Harrison, A. M. Randall and G. Ferguson, *J. Chem. Soc., Perkin Trans. 2*, 1991, 87–99.
10 E. T. Clarke and A. T. Martell, *Inorg. Chim. Acta*, 1991, **190**, 27–36.
11 E. T. Clarke and A. T. Martell, *Inorg. Chim. Acta*, 1991, **190**, 37–46.
12 J. Byegard, G. Skarnemark and M. Skalberg, *J. Radioanal. Nucl. Chem.*, 1999, **241**, 281–290.
13 H. R. Maecke, *Radiolabeled Peptides in Nuclear Oncology: Influence of Peptide Structure and Labeling Strategy on Pharmacology*, Ernst Schering Res Found Workshop, 2005, pp. 43–72.
14 H. R. Maecke, M. Hofmann and U. Haberkorn, *J. Nucl. Med.*, 2005, **46**, 172S–178S.
15 M. Halim, M. S. Tremblay, S. Jockusch, N. J. Turro and D. Sames, *J. Am. Chem. Soc.*, 2007, **129**, 7704–7705.
16 K. Hanaoka, K. Kikuchi, S. Kobayashi and T. Nagano, *J. Am. Chem. Soc.*, 2007, **129**, 13502–13509.
17 Available from Macrocyclics: http://www.macrocyclics.com/.
18 B. Wangler, C. Beck, U. Wagner-Utermann, E. Schirrmacher, C. Bader, F. Rosch, R. Schirrmacher and M. Eisenhut, *Tetrahedron Lett.*, 2006, **47**, 5985–5988.
19 L. M. De Leon-Rodriguez, Z. Kovacs, G. R. Dieckmann and A. D. Sherry, *Chem.–Eur. J.*, 2004, **10**, 1149–1155.
20 M. R. Lewis, F. Jia, F. Gallazzi, Y. Wang, J. Zhang, N. Shenoy, S. Z. Lever and M. Hannink, *Bioconjugate Chem.*, 2002, **13**, 1176–1180.
21 M. R. Lewis, J. Y. Kao, A.-L. J. Anderson, J. E. Shively and A. Raubitschek, *Bioconjugate Chem.*, 2001, **12**, 320–324.
22 J. J. Peterson, R. H. Pak and C. F. Meares, *Bioconjugate Chem.*, 1999, **10**, 316–320.
23 B. Yoo and M. D. Pagel, *Tetrahedron Lett.*, 2006, **47**, 7327–7330.
24 K. Tanaka, T. Masuyama, K. Hasegawa, T. Tahara, H. Mizuma, Y. Wada, Y. Watanabe and K. Fukase, *Angew. Chem., Int. Ed.*, 2008, **47**, 102–105.
25 K. Tanaka, M. Kamatani, H. Mori, S. Fujii, K. Ikeda, M. Hisada, Y. Itagaki and S. Katsumura, *Tetrahedron*, 1999, **55**, 1657–1686.
26 K. Tanaka, H. Mori, M. Yamamoto and S. Katsumura, *J. Org. Chem.*, 2001, **66**, 3099–3110.
27 K. Tanaka and S. Katsumura, *J. Am. Chem. Soc.*, 2002, **124**, 9660–9661.
28 K. Tanaka, T. Kobayashi, H. Mori and S. Katsumura, *J. Org. Chem.*, 2004, **69**, 5906–5925.
29 X. Chen, R. Park, M. Tohme, A. H. Shahinian, J. R. Bading and P. S. Conti, *Bioconjugate Chem.*, 2004, **15**, 41–49.
30 X. Chen, S. Liu, Y. Hou, M. Tohme, R. Park, J. R. Bading and P. S. Conti, *Mol. Imaging Biol.*, 2004, **6**, 350–359.
31 X. Chen, Y. Hou, M. Tohme, R. Park, V. Khankaldyyan, I. Gonzales-Gomez, J. R. Bading, W. E. Laug and P. S. Conti, *J. Nucl. Med.*, 2004, **45**, 1776–1783.
32 X. Chen, E. Sievers, Y. Hou, R. Park, M. Tohme, R. Bart, R. Bremner, J. R. Bading and P. S. Conti, *Neoplasia*, 2005, **7**, 271–279.
33 Y. Wu, X. Zhang, Z. Xiong, Z. Cheng, D. R. Fisher, S. Liu, S. S. Gambhir and X. Chen, *J. Nucl. Med.*, 2005, **46**, 1707–1718.
34 S. Froidevaux and A. N. Eberle, *Biopolymers*, 2002, **66**, 161–183.
35 A. Heppeler, S. Froidevaux, H. R. Macke, E. Jermann, M. Behe, P. Powell and M. Hennig, *Chem.–Eur. J.*, 1999, **5**, 1974–1981.
36 S. Froidevaux, A. N. Eberle, M. Christe, L. Sumanovski, A. Heppeler, J. S. Schmitt, K. Eisenwiener, C. Beglinger and H. R. Macke, *Int. J. Cancer*, 2002, **98**, 930–937.
37 K.-P. Eisenwiener, M. I. M. Prata, I. Buschmann, H.-W. Zhang, A. C. Santos, S. Wenger, J. C. Reubi and H. R. Macke, *Bioconjugate Chem.*, 2002, **13**, 530–541.
38 O. Ugur, P. J. Kothari, R. D. Finn, P. Zanzonico, S. Ruan, I. Guenther, H. R. Maecke and S. M. Larson, *Nucl. Med. Biol.*, 2002, **29**, 147–157.
39 M. R. Lewis, D. E. Reichert, R. Laforest, W. H. Margenau, R. E. Shefer, R. E. Klinkowstein, B. J. Hughey and M. J. Welch, *Nucl. Med. Biol.*, 2002, **29**, 701–706.
40 F. Rosch, H. Herzog, B. Stolz, J. Brockmann, M. Kohle, H. Muhlensiepen, P. Marbach and H.-W. Muller-Gartner, *Eur. J. Nucl. Med.*, 1999, **26**, 358–366.
41 M. Henze, J. Schuhmacher, P. Hipp, J. Kowalski, D. W. Becker, J. Doll, H. R. Macke, M. Hofmann, J. Debus and U. Haberkorn, *J. Nucl. Med.*, 2001, **42**, 1053–1056.
42 M. Henze, A. Dimitrakopoulou-Strauss, S. Milker-Zabel, J. Schuhmacher, L. G. Strauss, J. Doll, H. R. Macke, M. Eisenhut, J. Debus and U. Haberkorn, *J. Nucl. Med.*, 2005, **46**, 763–769.
43 S. Milker-Zabel, A. Z.-D. Bois, M. Henze, P. Huber, D. Schulz-Ertner, A. Hoess, U. Haberkorn and J. Debus, *Int. J. Radiat. Oncol., Biol., Phys.*, 2006, **65**, 222–227.
44 G.-J. Meyer, H. Macke, J. Schuhmacher, W. H. Knapp and M. Hofmann, *Eur. J. Nucl. Med. Mol. Imaging*, 2004, **31**, 1097–1104.
45 W. A. P. Breeman, M. de Jong, E. de Blois, B. F. Bernard, M. Konijnenberg and E. P. Krenning, *Eur. J. Nucl. Med. Mol. Imaging*, 2005, **32**, 478–485.
46 M. Rodrigues, T. Traub-Weidinger, M. Leimer, S. Li, F. Andreae, P. Angelberger, R. Dudczak and I. Virgolini, *Eur. J. Nucl. Med. Mol. Imaging*, 2005, **32**, 1144–1151.
47 F. Jamer, R. Barone, I. Mathieu, S. Walrand, D. Laber, P. Carlier, J. De Camps, H. Schran, T. Chen, M. C. Smith, H. Bouterfa, R. Valkema, E. P. Krenning, L. K. Kvols and S. Pauwels, *Eur. J. Nucl. Med. Mol. Imaging*, 2003, **30**, 510–518.
48 R. Barone, S. Pauwels, J. De Camps, E. P. Krenning, L. K. Kvols, M. C. Smith, H. Bouterfa, O. Devuyst and F. Jamar, *Nephrol. Dial. Transplant.*, 2004, **19**, 2275–2281.
49 X. Chen, R. Park, Y. Hou, M. Tohme, A. H. Shahinian, J. R. Bading and P. S. Conti, *J. Nucl. Med.*, 2004, **45**, 1390–1397.
50 B. E. Rogers, H. M. Bigott, D. W. McCarthy, D. D. Manna, J. Kim, T. L. Sharp and M. J. Welch, *Bioconjugate Chem.*, 2003, **14**, 756–763.
51 Y.-S. Yang, X. Zhang, Z. Xiong and X. Chen, *Nucl. Med. Biol.*, 2006, **33**, 371–380.
52 J. Schuhmacher, H. Zhang, J. Doll, H. R. Macke, R. Matys, H. Hauser, M. Henze, U. Haberkorn and M. Eisenhut, *J. Nucl. Med.*, 2005, **46**, 691–699.
53 S. Froidevaux, M. Calame-Christe, J. Schuhmacher, H. Tanner, R. Saffrich, M. Henze and A. N. Eberle, *J. Nucl. Med.*, 2004, **45**, 116–223.
54 P. McQuade, Y. Miao, J. Yoo, T. P. Quinn, M. J. Welch and J. S. Lewis, *J. Med. Chem.*, 2005, **48**, 2985–2992.
55 M. F. Giblin, N. Wang, T. J. Hoffman, S. S. Jurissson and T. P. Quinn, *Proc. Natl. Acad. Sci. U. S. A.*, 1998, **95**, 12814–12818.
56 I. Velikyan, A. L. Sundberg, O. Lindhe, A. U. Hoglund, O. Eriksson, E. Werner, J. Carlsson, M. Bergstrom, B. Langstrom and V. Tolmachev, *J. Nucl. Med.*, 2005, **46**, 1881–1888.
57 P. A. Schubiger, R. Alberto and A. Smith, *Bioconjugate Chem.*, 1996, **7**, 165–179.

58 T. Olafsen, V. E. Kenanova, G. Sundaresan, A.-L. Anderson, D. Crow, P. J. Yazaki, L. Li, M. F. Press, S. S. Gambhir, L. E. Williams, J. Y. C. Wong, A. A. Raubitschek, J. E. Shively and A. M. Wu, *Cancer Res.*, 2005, **65**, 5907–5916.
59 P. M. Smith-Jones, D. Solit, F. Afroze, N. Rosen and S. M. Larson, *J. Nucl. Med.*, 2006, **47**, 793–796.
60 P. M. Smith-Jones, D. B. Solit, T. Akhurst, F. Afroze, N. Rosen and S. M. Larson, *Nat. Biotechnol.*, 2004, **22**, 701–706.
61 A. M. Wu, P. J. Yazaki, S. Tsai, K. Nguyen, A.-L. Anderson, D. W. McCarthy, M. J. Welch, J. E. Shively, L. E. Williams, A. A. Raubitschek, J. Y. C. Wong, T. Toyokuni, M. E. Phelps and S. S. Gambhir, *Proc. Natl. Acad. Sci. USA*, 2000, **97**, 8495–8500.
62 M. R. Lewis, A. Raubitschek and J. E. Shively, *Bioconjugate Chem.*, 1994, **5**, 565–576.
63 J. Grunberg, I. Novak-Hofer, M. Honer, K. Zimmermann, K. Knogler, P. Blauenstein, S. Ametamey, H. R. Maecke and P. A. Schubiger, *Clin. Cancer Res.*, 2005, **11**, 5112–5120.
64 M. R. Lewis, M. Wang, D. B. Axworthy, L. J. Theodore, R. W. Mallet, A. R. Fritzberg, M. J. Welch and C. J. Anderson, *J. Nucl. Med.*, 2003, **44**, 1284–1292.
65 D. B. Axworthy, J. M. Reno, M. D. Hylarides, R. W. Mallet, L. J. Theodore, L. M. Gustavson, F.-M. Su, L. J. Hobson, P. L. Beaumier and A. R. Fritzberg, *Proc. Natl. Acad. Sci. U. S. A.*, 2000, **97**, 1802–1807.
66 G. J. Forster, E. B. Santos, P. M. Smith-Jones, P. Zanzonico and S. M. Larson, *J. Nucl. Med.*, 2006, **47**, 140–149.
67 K. Matsui, Z. Wang, T. J. McCarthy, P. M. Allen and D. E. Reichert, *Nucl. Med. Biol.*, 2004, **31**, 1021–1031.
68 J. Hoffend, W. Mier, J. Schuhmacher, K. Schmidt, A. Dimitrakopoulou-Strauss, L. G. Strauss, M. Eisenhut, R. Kinscherf and U. Haberkorn, *Nucl. Med. Biol.*, 2005, **32**, 287–292.
69 W. Mier, J. Hoffend, S. Kramer, J. Schuhmacher, W. E. Hull, M. Eisenhut and U. Haberkorn, *Bioconjugate Chem.*, 2005, **16**, 237–240.
70 K. Schmidt, J. Hoffend, A. Altmann, L. G. Strauss, A. Dimitrakopoulou-Strauss, B. Engelhardt, D. Koczan, J. Peter, T. J. Dengler, W. Mier, M. Eisenhut, U. Haberkorn and R. Kinscherf, *J. Nucl. Med.*, 2006, **47**, 543–551.
71 K. Schmidt, J. Hoffend, A. Altmann, F. Kiessling, L. G. Strauss, D. Koczan, W. Mier, M. Eisenhut, R. Kinscherf and U. Haberkorn, *J. Nucl. Med.*, 2006, **47**, 1506–1514.
72 A. Roivainen, T. Tolvanen, S. Salomaki, G. Lendvai, I. Velikyan, P. Numminen, M. Valila, H. Sipila, M. Bergstrom, P. Harkonen, H. Lonnberg and B. Langstrom, *J. Nucl. Med.*, 2004, **45**, 347–355.
73 G. Lendvai, I. Velikyan, M. Bergstrom, S. Estrada, D. Laryea, M. Valila, S. Salomaki, B. Langstrom and A. Roivainen, *Eur. J. Pharm. Sci.*, 2005, **26**, 26–38.
74 K. Kita, S. Saito, C. Y. Morita and A. Watanabe, *Int. J. Cancer*, 1999, **80**, 553–558.
75 X. Sun, H. Fang, X. Li, R. Rossin, M. J. Welch and J. S. Taylor, *Bioconjugate Chem.*, 2005, **16**, 294–305.
76 A. G. Morell, R. A. Irvine, I. Sternlieb, I. H. Scheinberg and G. Ashwell, *J. Biol. Chem.*, 1968, **243**, 155–159.

